Chapter 6
MEIS Study of the Initial Growth of Fe on Si(111)

6.1   Introduction

Fe silicides have attracted much recent attention due to their direct band gap of ~0.85 eV [1, 2] and potential applications in the electronics industry [3-5]. Depending on the exact Fe:Si composition several phases may be formed which have been seen to exhibit semiconducting or metallic properties [6-14]. Despite this attention the Fe silicide system is still not fully understood, the bulk phase diagram being complex (Figure 6.1) [15]. This is particularly true of low Fe coverage on the clean Si surface, which is relevant for the possible integration of such silicides with current electronics. The formation of the iron–silicon interface is also of relevance to the possible application of Fe silicide in spin electronics
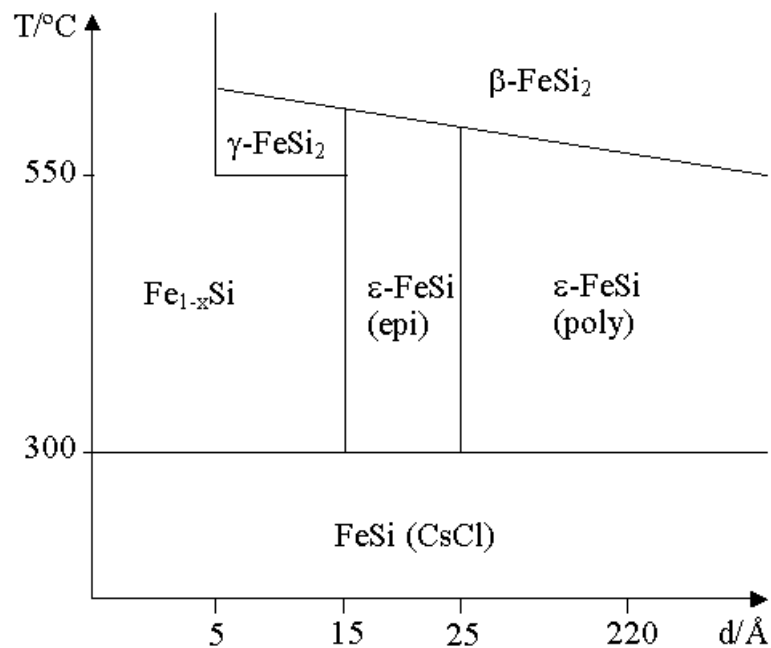

Figure 6.1: Bulk phase diagram for Fe silicide. After von Kanel et al. [15]. The FeSi system exhibits many phases in the bulk dependent on the precise Fe:Si composition and sample preparation.

(or "spintronics" as it has become known). One of the major problems within this rapidly developing field is the injection of spin polarised electrons into a semiconductor. One approach relies on a ferromagnetic layer to supply the spin polarised electrons. Fe silicides are obvious potential candidates for this ferromagnetic layer. Indeed, the first room temperature injection of spin polarised electrons into a semiconductor was demonstrated with Fe on GaAs [16]. However the Fe silicide–silicon interface is generally somewhat rough [7] which degrades efforts into spin injection from such a layer. A better understanding of the initial Fe growth ought to allow for a smoother interface to be developed.

In the context of the current body of work a MEIS study of the initial growth of Fe on the clean Si(111) surface was undertaken due to the interests as outlined above and as a precursor to the investigation of Fe growth on the 2D silicides described in previous chapters. In fact an initial investigation of such growth is briefly presented in the next chapter. The interpretation of Fe growth on 2D silicides would be greatly aided by a fuller understanding of the growth of Fe on Si.

6.2   Experimental Details

The MEIS experiments were performed at the CCLRC Daresbury Laboratory MEIS facility described in Chapter 2. Samples were prepared *in situ* under UHV conditions at a base pressure of around 1×10^{-10} mbar. Lightly doped, 100 Ω cm, *n*-type Si(111) wafers were cut into approximately 1×1 cm^2 samples. The samples were introduced into the UHV system and cleaned by repeated electron beam bombardment flash heating to 1200 ˚C followed by a slow (<100 ˚C/min) cool to room temperature. The temperature of the samples was monitored by means of an infra red pyrometer external to the vacuum chamber. The cleaned Si(111) samples produced a characteristic sharp 7×7 LEED pattern and AES showed no indication of surface contamination.

Fe was deposited onto the room temperature samples using an in house designed source consisting of a simple Fe wire heated by means of the passing of electrical current (15–20 A) through it. The pressure during this deposition remained below 1×10^{-9} mbar. Deposition rates were estimated from the MEIS spectra of as deposited samples. After deposition AES was used to ensure a lack of contamination (especially due to oxygen) and only a diffuse background was apparent from LEED. The samples were gently e⁻-beam annealed to around 300 ˚C, where upon a 1×1 LEED pattern could be observed. Further e⁻-beam annealing to about 500 ˚C produced a 2×2 LEED pattern. Such an evolution has been reported before (see for example Starke *et al*. [12] and Urano *et al*. [17, 18], though the structure is unclear). The 2×2 pattern could also be obtained from the freshly deposited samples by annealing to 500 ˚C without the intermediate anneal to 300 ˚C.

Once prepared in such a way the samples were transferred within the UHV system to the MEIS scattering chamber. A 100 keV H^+ ion beam was used in low index double alignment MEIS experiments. The beam dose was 10^{16} ions cm⁻² and the size of the beam at the sample approximately 0.5 mm × 1 mm normal to the beam. In order to minimise sample damage the samples were moved vertically, maintaining the double alignment geometry, between acquiring data sets. Three double aligned scattering geometries were employed: [$\bar{1}$ 00] incidence with detection around [$\bar{1}$ 11]; [1$\bar{1}$ $\bar{1}$] incidence with detection around [100]; and [1$\bar{1}$ 0] incidence with detection around [100].

6.3   Results and Discussion

6.3.1   *Experimental Data*

Typical MEIS spectra from the three scattering geometries are shown in Figure 6.2 and Figure 6.3. The mass separation effects are evident, allowing the signals from ions scattered from the Fe and Si to be clearly resolved, as indicated. Scattered ions with energy lower than those of the Si signal have been scattered
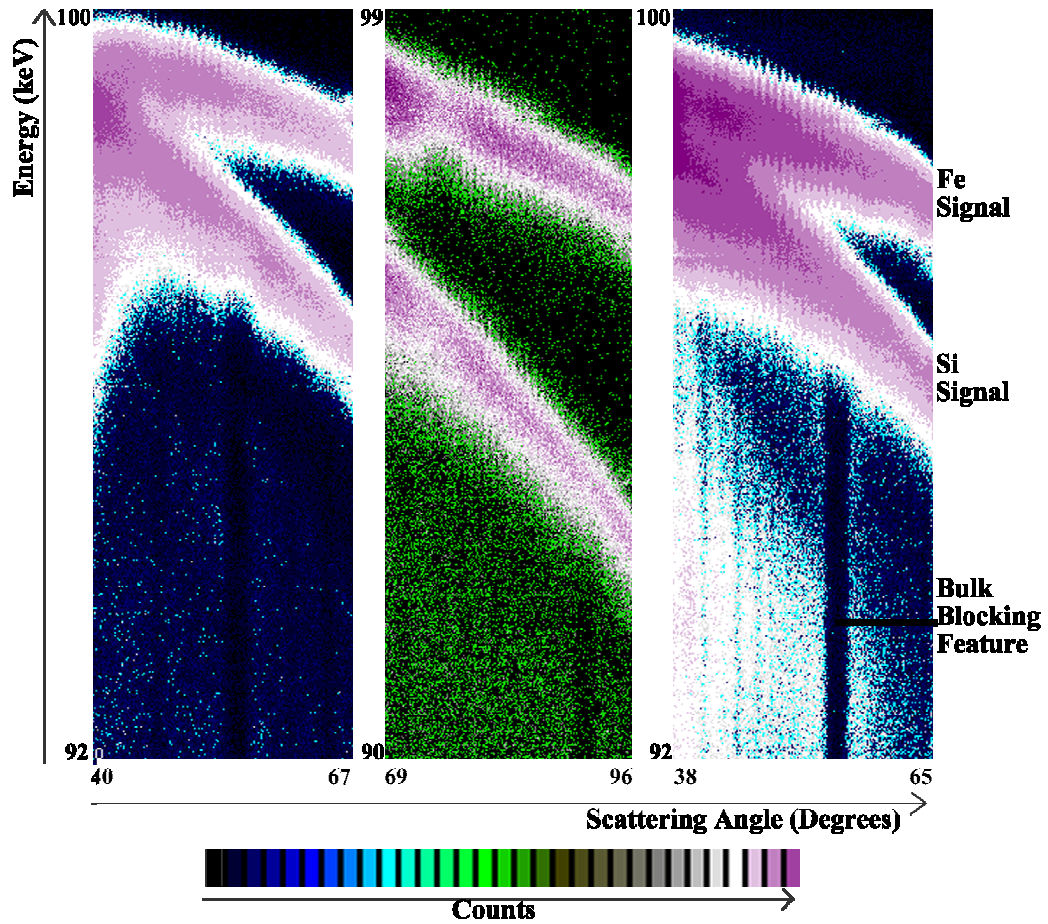
Original in colour

Figure 6.2: Typical MEIS spectra from the FeSi 1 × 1 phase. Left to right: [$\bar{1}$00]/[$\bar{1}$11], [1$\bar{1}$0]/[100], [1$\bar{1}$ $\bar{1}$]/[100]. The Fe signal shows clear blocking dips.
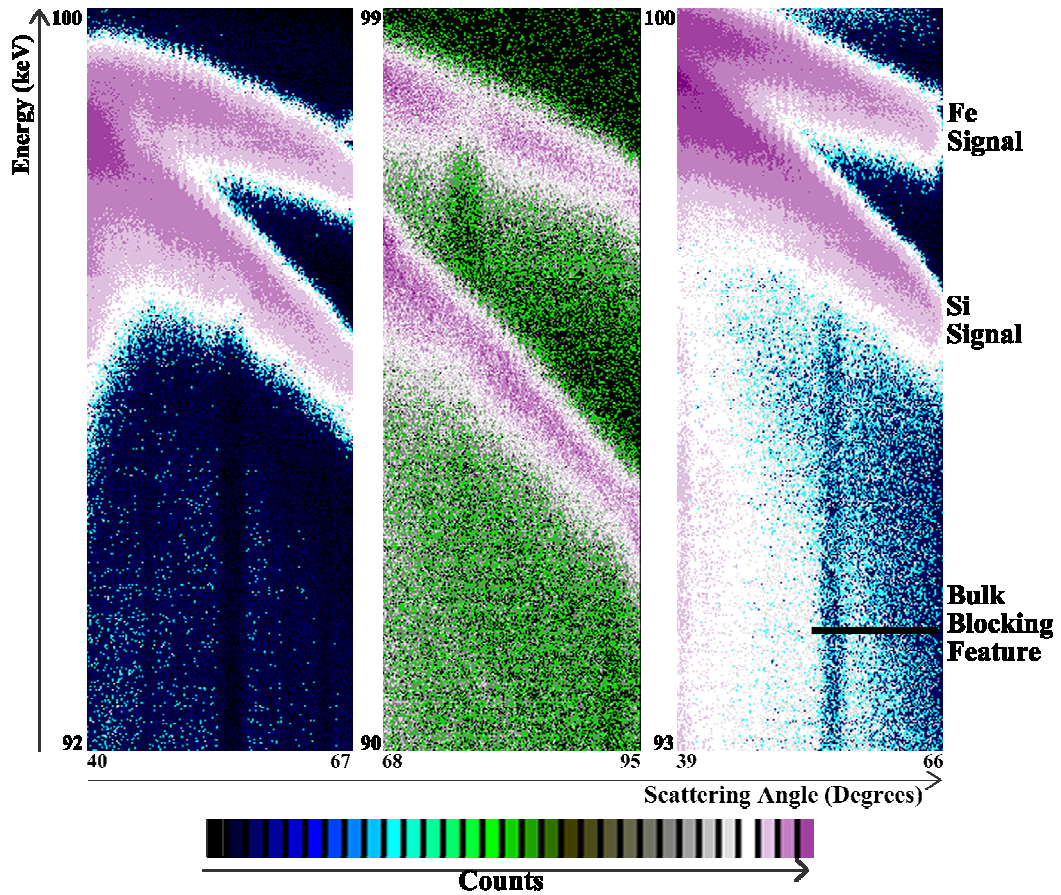
Original in colour

Figure 6.3: Typical MEIS spectra from the FeSi 2 × 2 phase. Left to right: [Ī 00]/[Ī 11]; [1Ī 0]/[100]; [1Ī Ī]/[100]. The spectra are very similar to those observed for the 1 × 1 phase (Figure 6.2).

from the bulk Si. The main blocking dip in this bulk signal was used to calibrate the angular scale of the spectra correcting, for example, for any mechanical offset in the detector position. This was achieved by integrating the scattered ion count as a function of angle over the energy range corresponding to the bulk signal. The scattering curve so produced was then compared to a Monte Carlo computer simulation produced using the VEGAS code [19, 20] (see Chapter 3), of the scattering from bulk terminated Si and the blocking features examined. This allowed an angular shift to be determined to bring the blocking features into alignment and thus calibrate the angular scale.

The scattered ion count was similarly integrated as a function of angle over the energy range of the ions scattered from the Fe. This curve was then shifted by the angular offset determined from the bulk calibration procedure described above. The data was also corrected for the kinetic energy loss factor and the fall off in counts with scattering angle due to the Rutherford scattering cross section (the reader is directed to Chapter 3 for a fuller description of these effects).

The corrected scattering curves for both the 1×1 and 2×2 reconstructions are compared in Figure 6.4, Figure 6.5 and Figure 6.6. It is immediately apparent that the scattering curves from the two phases are extremely similar. This is consistent with the hypothesis that the 2×2 reconstruction is due to an ordered Si overlayer. Such a 2×2 overlayer would consist of ¼ monolayer (ML) of Si adatoms, which may be expected to contribute little to the blocking curves. However, this small contribution cannot in itself explain the similarity. It is also proposed that in these scattering geometries the 2×2 adatoms are effectively shadowed from the scattered ions by the layers below them.
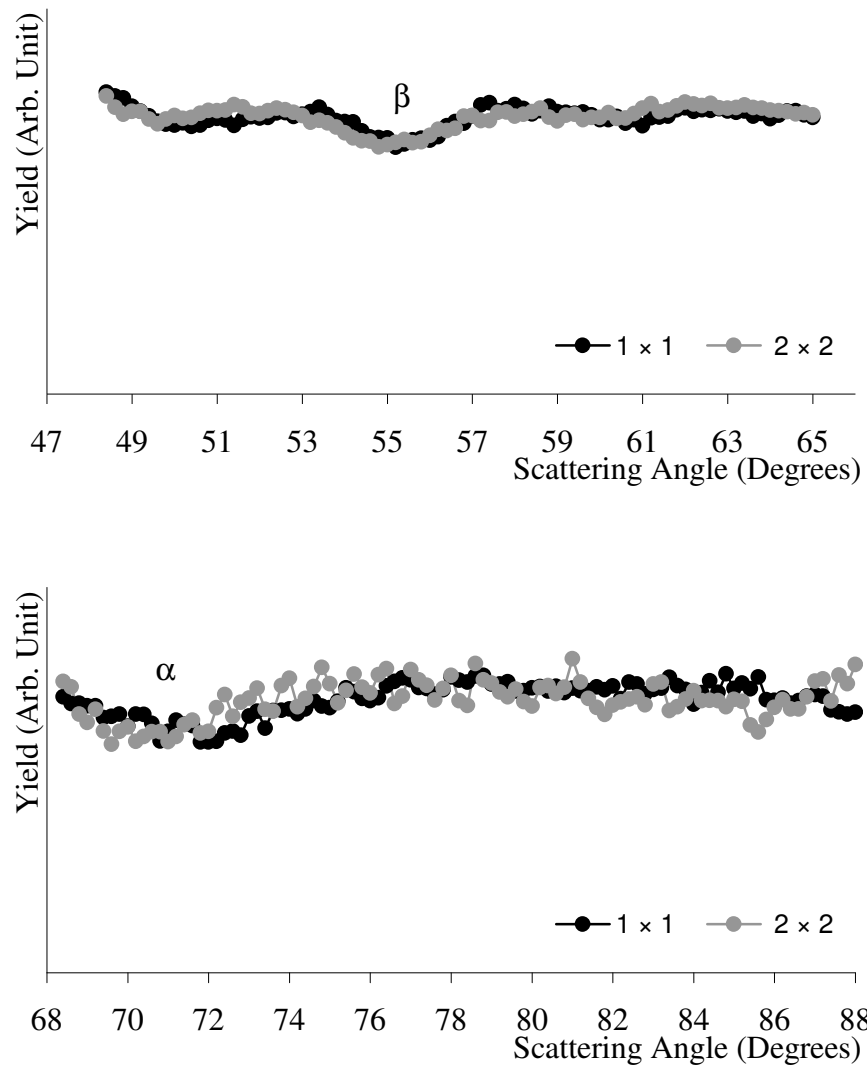
Figure 6.4: Comparison of scattering curves from the 1 × 1 and 2 × 2 phases. [Ī 00]/[Ī 11] geometry. The scattering curves from the two phases are extremely similar, indicating that their structures are very alike. See also Figure 6.5 and Figure 6.6.
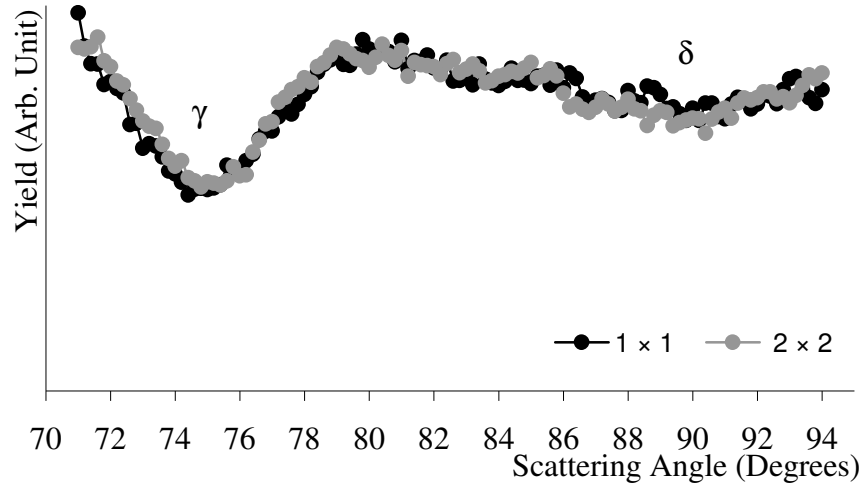
Figure 6.5: Comparison of scattering curves from the 1 × 1 and 2 × 2 phases. [1Ī 0]/[100] geometry. See also Figure 6.4 and Figure 6.6.
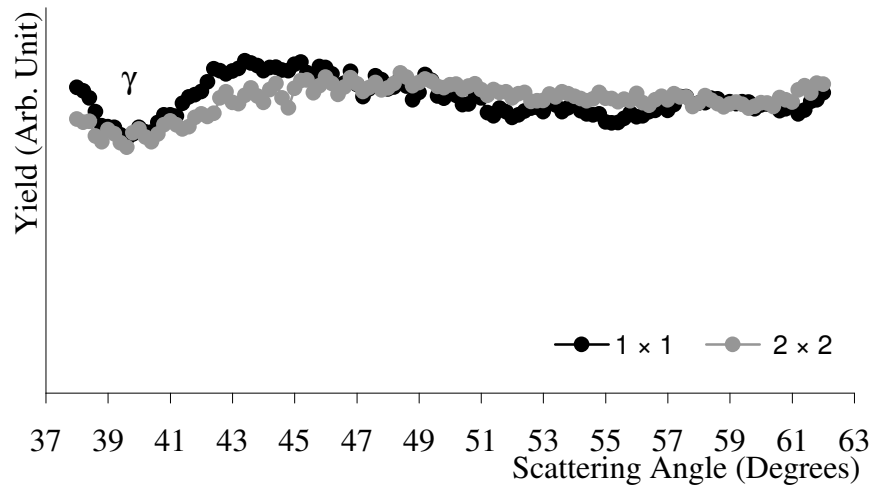

Figure 6.6: Comparison of scattering curves from the 1 × 1 and 2 × 2 phases. [1Ī Ī]/[100] geometry. See also Figure 6.4 and Figure 6.5.

132

6.3.2   Possible Models

Bulk Fe silicides have a CsCl or CaF_2 type structure depending on the composition and anneal conditions. Based on geometric considerations of the position of blocking features in the Fe scattering curve several possible models for the Fe silicide were devised deriving from these structural types. Monte Carlo computer simulations of ion scattering from the Fe in these models were performed using the VEGAS codes, initially concentrating on just a 1×1 reconstruction.

From these simulations it was immediately apparent that there could be at most two Fe layers within the silicide. The introduction of a third or further, deeper, layers would introduce many more blocking features into the scattering curve than observed. This conclusion is consistent with the estimated Fe coverage of 1.7 ML which would imply at most two layers of Fe. It is noted here that for a single Fe layer there is no distinction between a CsCl- and CaF_2-type structure.

The simple CsCl- or CaF_2-type structures first modelled were found to be unable to reproduce the blocking features observed. Further careful consideration of the blocking features led to the construction of a model in which a CsCl-type Fe silicide layer has a "B-type" orientation with respect to the bulk Si, i.e. the "buckling" direction of the Fe silicide is reversed compared to that of the bulk Si. This model is shown in Figure 6.7. Such B-type orientated Fe silicide growth has been noted before [21-25]. Note that as the signal from Fe scattering was analysed the registration to the bulk Si, below the Fe, is unknown.

Figure 6.7 shows the 2×2 arrangement of Si adatoms. It is proposed that the 1×1 phase observed at lower anneal temperatures is identical but lacks this ordered 2×2 overlayer, though the extreme similarity of the blocking curves suggests that an unordered overlayer may be present with some Si atoms in T4 sites. Figure 6.8 shows the origin of the major blocking features in the three
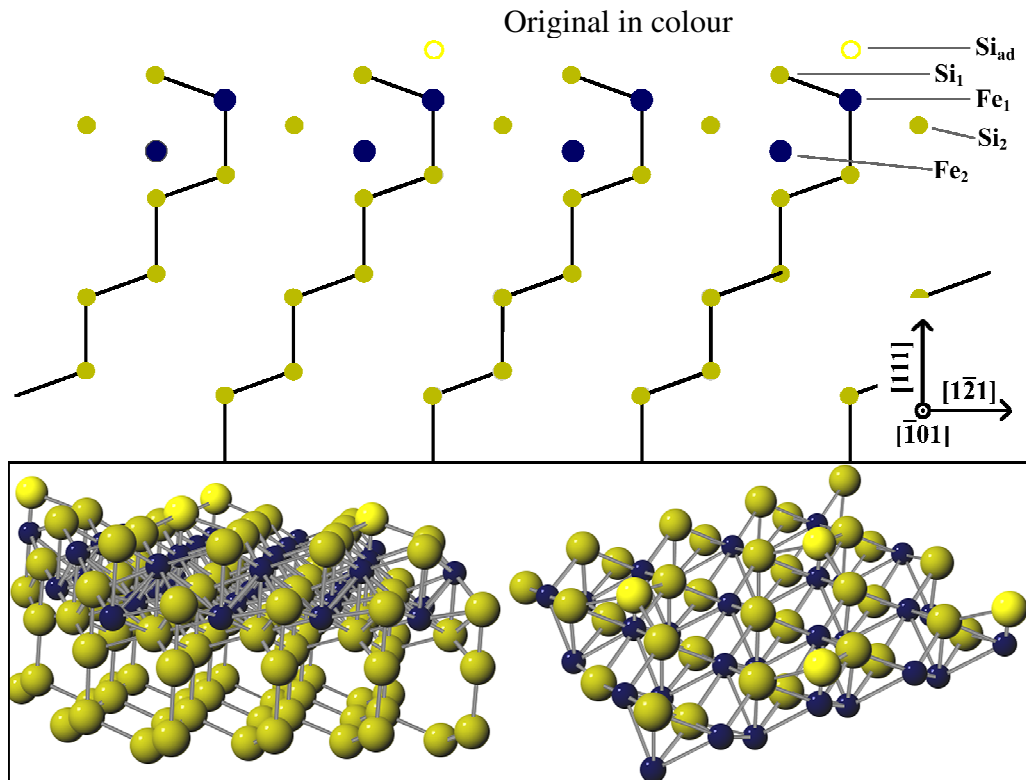
133

Original in colour

Figure 6.7: The proposed structural model for the initial Fe silicide growth. Side view showing the scattering plane. Note that the 2 × 2 phase is shown; the 1 × 1 phase is proposed to be identical but without the ordered Si overlayer, Si_{ad}. Inset: Ball and stick model of the surface—the model on the right has the bulk Si removed for clarity.

geometries for which data was available. It can be seen that the 2 × 2 arrangement of adatoms is mainly shadowed from the scattered ions.

6.3.3   *Optimising Structural Parameters*

A number of multicalc simulations were performed allowing the vertical heights of Si_{ad}, Si_1, Fe_1 and Si_2 to vary. The thermal vibrations of the atoms were estimated from the Debye temperatures [26] to give root mean square (rms) vibrational amplitudes of 0.08 Å. In order to adequately fit the size of the blocking curves it was necessary to develop a model in which the silicide contained 1 or 2 Fe layers in an equal ratio. i.e. half the surface covered with the silicide as shown in Figure 6.7 and the other half with the silicide lacking the Fe_2

layer. This is consistent with the estimated Fe coverage of 1.7 ML.

The analysis of the simulations was simplified by careful consideration of the origin of the blocking features. The feature labelled α in Figure 6.8 is due only to blocking by Fe_1 atoms of ions scattered from Fe_2. Therefore adjustment of the Fe_1 height, relative to Fe_2, to fit this blocking feature in the simulations allows the vertical separation of the two Fe layers to be fixed. The feature marked β could then be used to fix the vertical position of Si_1 and Si_{ad}—Si_{ad} must be at such a height as to remain in the shadow cone cast by the Si_1 atoms. The position of Si_1 could be confirmed from the γ feature. This blocking dip could also be used to determine the position of the Si2 atoms. Finally the δ blocking dip
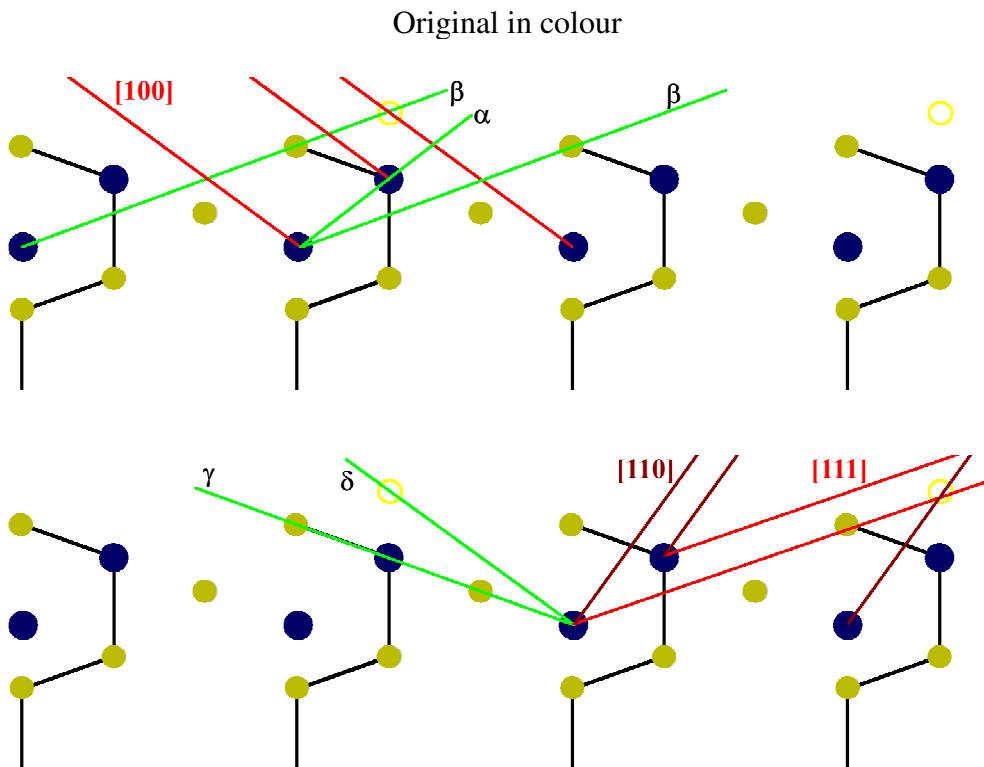
Original in colour

Figure 6.8: Origin of the blocking features. Note how the adatoms are mainly shadowed from the scattered ions. Red lines indicate the incident ion directions, green lines the origin of the observed blocking dips Top: [Ī 00]/[Ī 11] Bottom: [1Ī 0]/[100] and [1Ī Ī]/[100]—as ions are detected around [100] in both cases the same blocking dips are observed, although at different scattering angles.

135

confirms the position of the adatom. This feature is, however, weak due to it being only a $^1/_8$ monolayer contribution (the 2×2 adatom arrangement represents a $^1/_4$ monolayer but the blocking feature involves scattering from the second layer Fe, which is present in only half the surface area). In the case of the $[1\bar{1}\ \bar{1}\ ]/[100]$ geometry the feature is weakened still further by the shadowing of the second layer Fe by the Si_1 atoms.

Comparisons of simulated scattering curves to the experimental data are presented in Figure 6.10, Figure 6.11, and Figure 6.12, for the 2×2 case. The structural parameters of this best fit model are given in Table 6.1 and shown in Figure 6.9. The Fe–Si bond lengths derived from this model are comparable to those for bulk Fe silicides (2.40 Å). The Si_{ad}–Si_1 bond length is slightly contracted compared to the Si–Si bond length of bulk Si (2.35 Å).

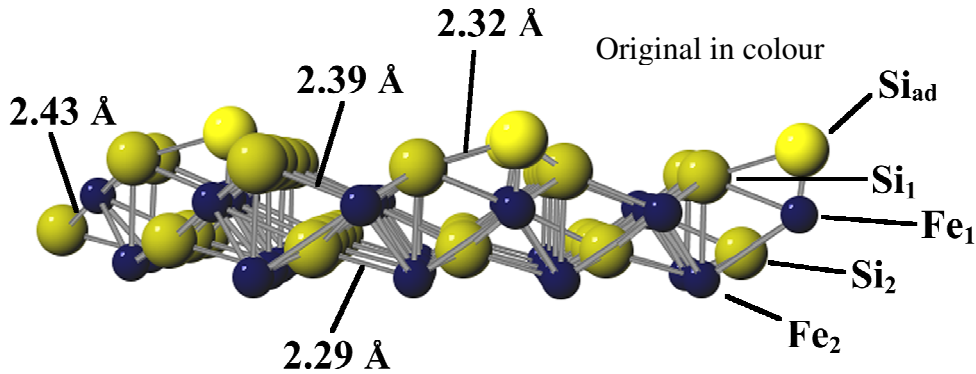*Figure 6.9: Ball and stick model of the surface, showing the bond lengths detailed in Table 6.1.*

	Si_{ad}–Si_1 (Å)	Si_1–Fe_1 (Å)	Fe_1–Si_2 (Å)	Si_2–Fe_2 (Å)
Vertical Distance	0.68 ± 0.05	0.88 ± 0.02	0.98 ± 0.04	0.58 ± 0.04
Bond Length	2.32 ± 0.03	2.39 ± 0.01	2.43 ± 0.02	2.29 ± 0.02

Table 6.1: Structural parameters for the final model. See Figure 6.7 for labels.

Original in colour

Figure 6.10: Comparison of simulated and experimental scattering curves for the final structural model. The [Ī 00]/[Ī 11] geometry.
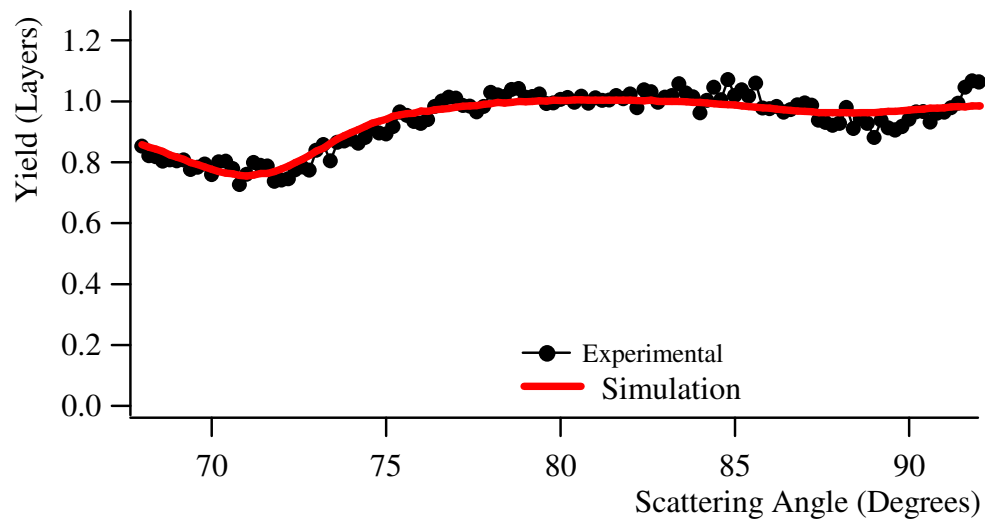
Original in colour

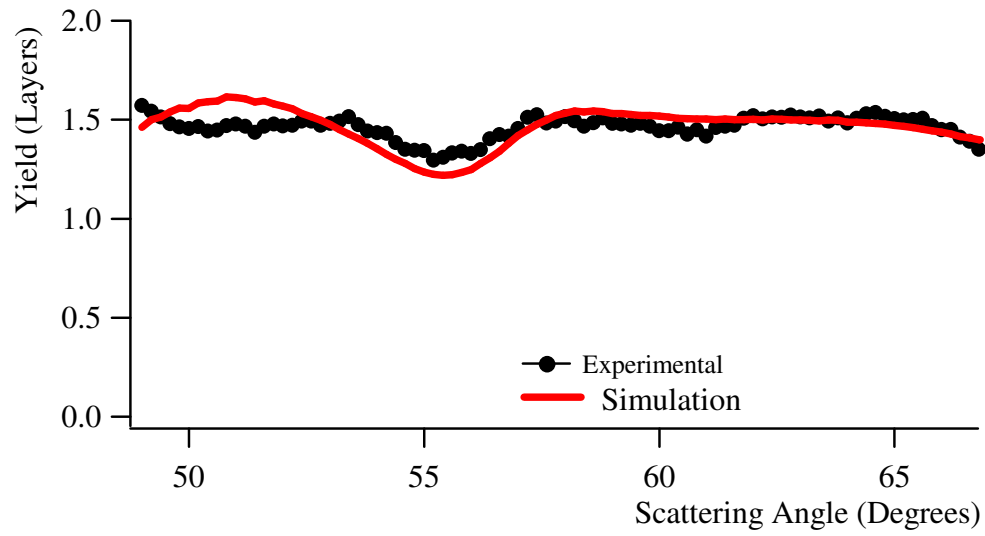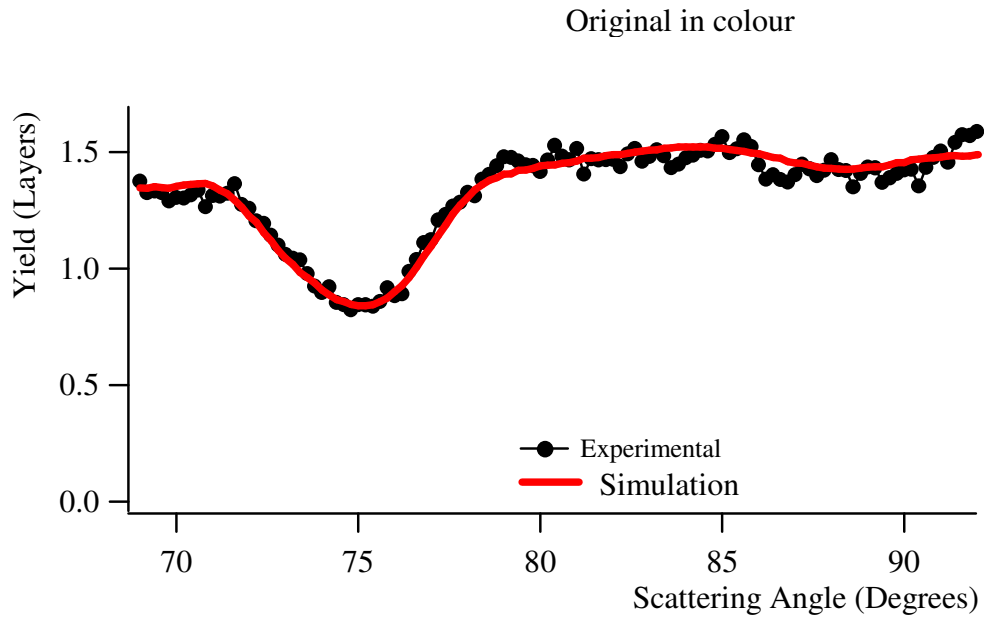*Figure 6.11 Comparison of simulated and experimental scattering curves for the final structural model. The [1$\bar{1}$ 0]/[100] geometry.*
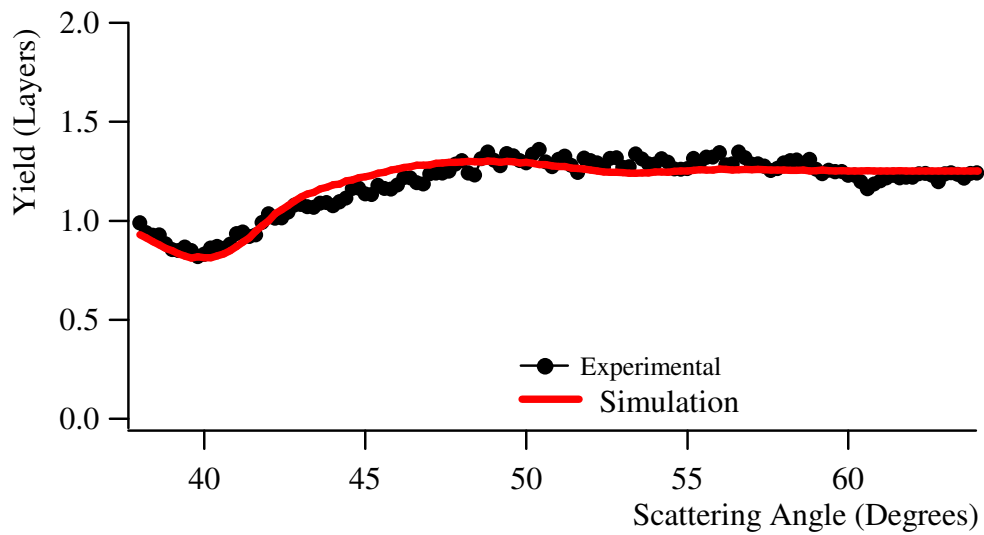

Figure 6.12: Comparison of simulated and experimental scattering curves for the final structural model. The [1$\bar{1}$ $\bar{1}$]/[100] geometry.

6.4   Conclusions

The initial growth of Fe on the Si(111) 7×7 surface has been studied by medium energy ion scattering. Depending upon the anneal conditions two possible phases have been formed. These phases exhibit a 1×1 reconstruction and a 2×2 reconstruction, as shown by LEED. The MEIS data shows the two phases to be extremely similar structurally, with very little difference in the blocking curves obtained from each phase.

It is proposed that the 2×2 phase is formed by the addition of a 2×2 overlayer of Si atoms, which are effectively shadowed from the scattered ions in this case. The structural model proposed consists of a B-type Fe silicide a with CaF_2 type structure. The adatoms rest in T4 sites above the first Fe layer, the Si–Si bond direction reverting to that of the bulk Si. To satisfactorily fit the observed blocking curves it was necessary to propose that the surface consisted of such a silicide with one and two Fe layers in equal proportion.

The structural model suggested could be confirmed with further MEIS data. While scattering data from slightly lower scattering angles within the scattering geometries used would provide further blocking features such data is not quite so readily obtained. At such low scattering angles the mass separation between the Fe and Si decreases making it difficult to extract the blocking curve from only one element. It is also important to maintain a bulk Si blocking feature within the data tile in order to calibrate the angular scale. A more rewarding approach may be to select a different scattering geometry, such as with the beam normal to the sample surface.

The surface also represents an ideal candidate for study by STM. The 2×2 Si overlayer would be apparent in STM images. STM may also reveal if there are indeed Si atoms within the T4 sites, but unordered, in the 1×1 phase as suggested by the similarity of the scattering curves.

This investigation of the initial formation of Fe silicide on the Si(111) 7×7 surface has resulted in a better understanding of the structures involved. This work may be used as a ba se for development of this understanding and also as an aid to understanding the interaction of Fe with more complex interfaces such as those formed by 2D silicides.

References

1.   M. De Crescenzi, G. Gaggiotti, N. Motta, F. Patella, A. Balzarotti and J. Derrien, *Phys. Rev. B* **42** 5871 (1990)

2.   N. E. Christensen, *Phys. Rev. B* **42** 7148 (1990)

3.   T. Ehara, S. Nakagomi and Y. Kokubun, *Solid-State Electron.* **47** 353 (2003)

4.   H. T. Lu, L. J. Chen, Y. L. Chueh and L. J. Chou, *J. Appl. Phys.* **93** 1468 (2003)

5.   D. Leong, M. Harry, K. J. Reeson and K. P. Homewood, *Nature* **387** 686 (1997)

6.   H. Moritz, B. Rösen, S. Popovic, A. Rizzi and H. Lüth, *Mat. Sci. Eng. B* **10** 1704 (1992)

7.   J. de la Figuera, A. L. V. De Parga, J. Alverez, J. Ibanez, C. Ocal and R. Miranda, *Surf. Sci.* **264** 45 (1992)

8.   W. Raunau, H. Niehus, T. Schilling and G. Comsa, *Surf. Sci.* **286** 203 (1993)

9.   A. L. V. De Parga, J. de la Figuera, C. Ocal and R. Miranda, *Ultramicroscopy* **42-44** 845 (1992)

10. H. von Känel, R. Stalder, H. Sirringhaus, N. Onda and J. Henz, *Appl. Surf. Sci.* **53** 196 (1991)

11. U. Kafader, P. Wetzel, C. Pirri and G. Gewinner, *Appl. Phys. Lett.* **63** 2360 (1993)

12. U. Starke, W. Weiss, M. Kutschera, R. Bandorf and K. Heinz, *J. Appl. Phys.* **91** 6154 (2002)

13. X. Wallart, H. S. Zeng, J. P. Nys and G. Dalmai, *Appl. Surf. Sci.* **56-58** 427 (1992)

14. J. Alvarez, A. L. Vázquez de Parga, J. J. Hinarejos, J. de la Figuera, E. G. Michel, C. Ocal and R. Miranda, *J. Vac. Sci. Technol. A* **11** 929 (1993)

15. H. von Kanel, N. Onda, H. Sirringhaus, E. Muller-Gubler, S. Goncalces-Conto and C. Schwarz, *Appl. Surf. Sci.* **70/71** 559 (1993)

16. H. J. Zhu, M. Ramsteiner, H. Kostial, M. Wassermeier, H. -P. Schönherr and K. H. Ploog, *Phys. Rev. Lett.* **87** 016601 (2001)

17. T. Urano and T. Kanaji, *Appl. Surf. Sci.* **33/34** 68 (1988)

18. T. Urano, M. Kaburagi, S. Hongo and T. Kanaji, *Appl. Surf. Sci.* **41/42** 103 (1989)

19. R. M. Tromp and J. F. van der Veen, *Surf. Sci.* **133** 159 (1983)

20. J. F. van der Veen, *Surf. Sci. Rep.* **5** 199 (1985)

21. U. Kafader, C. Pirri, P. Wetzel and G. Gewinner, *Appl. Surf. Sci.* **64** 297 (1993)

22.   S. Walter, R. Bandorf, W. Weiss, K. Heinz, U. Starke, M. Strass, M. Bockstedte and O. Pankratov, *Phys. Rev. B* **67** 085413 (2003)

23.   S Walter, F Blobner, M Krause, S Müller, K Heinz and U Starke, *J. Phys. Condens. Matter* **15** 5207 (2003)

24.   H. Sirringhaus, N. Onda, E. Müller–Gubler, P. Müller, R. Stalder and H. von Känel, *Phys. Rev. B* **47** 10567 (1993)

25.   S. Hong, C. Pirri, P. Wetzel, D. Bolmont and G. Gewinner, *Appl. Surf. Sci.* **90** 65 (1995)

26.   D. P. Woodruff and T. A. Delchar, *Modern Techniques of Surface Science*, Cambridge University Press (1986)